J Seismol (2016) 20:305–318
DOI 10.1007/s10950-015-9528-6

ORIGINAL ARTICLE

A preliminary one-dimensional crustal velocity model for Himachal Pradesh, India

Mahesh Prasad Parija · Sushil Kumar · Shubhasmita Biswal · Narendra Kumar · Saurabh Kumar Mishra

Received: 6 July 2015 / Accepted: 23 September 2015 / Published online: 9 October 2015

Abstract A preliminary one-dimensional (1D) velocity model for Himachal Pradesh, India has been developed by utilising the P and S wave travel time data. A very steady and narrow velocity model was obtained with travel time inversion, and a range of velocity models were tested with earthquake locations to derive the best-fit velocity model. The 1D velocity model proposed for the study region has seven uniform layers with interfaces at depths of 0, 5, 10, 15, 20, 25 and 30 km with P wave velocity of 5.219, 5.314, 5.391, 5.392, 5.964, 6.071 and 6.073 km/s and S wave velocity of 2.998, 3.015, 3.134, 3.135, 3.441, 3.482 and 3.647 km/s, respectively. According to the proposed model, the Moho in this part of the Himalaya lies at 60 km depth on an average. For P and S waves, the station correction ranges from −0.88 to 1.50 and −0.58 to 3.59 s, respectively. This low variation in station residuals indicates small lateral velocity changes that confirm the accuracy and stability of the proposed 1D velocity model. Using the new derived 1D velocity model, the earthquake epicentres were relocated and we observe a shallow seismic activity in the region at <30 km depth that clearly describes the ongoing convergence of the India-Eurasia plates in the study region. This study also infers a new, highly active seismic window in the latitude range of 31.8 °N to 32.8 °N and longitude range of 76.8 °E to 78.8 °E in the study region across the Kaurik-Chango fault, a causative fault for the 1975 Kinnaur earthquake.

Keywords Himachal Pradesh · Seismicity · 1D velocity model · Seismotectonics

M. P. Parija (✉) · S. Kumar · N. Kumar
Wadia Institute of Himalayan Geology, Dehradun, India
e-mail: maheshparija@gmail.com

S. Kumar
e-mail: sushil_rohilla@yahoo.co.in

N. Kumar
e-mail: narenbhu@gmail.com

S. Biswal
Indian Institute of Technology Kharagpur, Kharagpur, India
e-mail: susmitabiswal123@gmail.com

S. K. Mishra
University of Mysore, Mysore, India
e-mail: saurabhmishra71@gmail.com

1 Introduction

Seismic velocity is an important parameter in the assessment of regional tectonics and earthquake hazards and provides evidence of the evolutionary model of the Himalaya. Earlier studies show that the Himalayan arc system is prone to intense seismicity due to collision of the Indian and Eurasian plates at the northern boundary of India. There is also evidence of clustered seismicity between the Main Boundary Thrust (MBT) and Main Central Thrust (MCT) which illustrates the significant complexities in the tectonics of the region (Ni and Barzangi, 1984). Collision between India and Eurasia increased sufficient amount of strain accumulation in the northern part of the Indian plate, and the pre-

accumulated strain is released along the entire Himalayan arc system. The collection of small-scale earthquake data through temporary networks confirms such concentration of seismicity and wide variation in earthquake focal mechanisms in different parts of the Himalayan region (Pandey et al., 1995; Kayal et al., 2003; Bollinger et al., 2004). Himalayan arc comprises of regions of well-defined high/low seismicity, seismic gaps and tectonically stable zones (Khattri and Tyagi, 1983; Gaur et al., 1985; Srivastva et al., 1986; Khattri et al., 1989; Kayal, 2001; Kayal et al., 2003). It consists of five major faults, which are named as Indus-Tsangpo Suture Zone (ITSZ), South Tibetan Detachment (STD), MCT, MBT and Himalayan Frontal Thrust (HFT) of NW-SE trend. These major thrust faults and their associated fault systems are the centre of high magnitude of the past earthquakes like the Kangra earthquake of 1905 with magnitude $M_l \geq 7.8$ and Kinnaur earthquake of 1975 with $M_l \geq 6.8$ in Himachal Pradesh, India. The presence of the epicentres of the above two earthquakes shows that this region of the Himalaya is highly active and sensitive towards more devastating earthquakes.

Due to the absence of an efficient local velocity model along with poor azimuthal coverage of earlier seismic stations, it is quite difficult to understand the crustal structure and clustered seismicity patterns which further inhibits understanding the associated tectonics of the area. In order to provide a local seismic velocity model to improve the epicentral locations as well as to understand the seismicity and its tectonic implications for the Himachal region (NW Himalaya), a seismic array of 12 broadband stations was deployed in 2004 by the Wadia Institute of Himalayan Geology (WIHG), Dehradun. This array was further upgraded with 10 more broadband seismic stations in the Sutlej valley, Kinnaur. These two arrays of seismic stations operated during the period from 2004 to 2013 in and around the source region of 1905 Kangra and 1975 Kinnaur earthquake.

During this period, 476 local events having a least square residual error and good azimuthal gap were recorded. Subsequently, these events were analysed with a well-established technique of real-time inversion for hypocentre determination and crustal velocity structure. Hypocentre relocation achieved using the first-hand one-dimensional (1D) velocity model is more refined and has been quite helpful in explaining the complex tectonics of the region.

2 Tectonics and geology of the study area

Himachal Pradesh is surrounded with the state of Jammu and Kashmir in the northwest, Uttarakhand in the southeast and Tibet in the eastern side. Our study area in Kangra region, marked by three faults Chenab normal fault, Panjal thrust and Chamba thrust, is covered with weakly metamorphosed sediments and in the Kinnaur region is covered with medium to high grade metamorphic rocks emplaced with granitic intrusion of different ages of Vaikrita and Haimanta groups. The tectonic activity in this part of the Himalaya is due to the subduction of northward moving Indian plate under the Eurasian plate at the boundary called as ITSZ, and the current convergence of these two tectonic plates is marked by thrust mechanism. Due to this convergence of Indian plate with the adjacent Eurasian plate, the South Tibetan Detachment fault having a NW-SE trend is extending towards the south. Hence it causes a compression to Higher Himalayan Crystalline (HHC) (Thakur et al., 1995). As a result of this, a large number of tectonic and high-frequency seismic events are clustered in the Himalaya region. This compression gave rise to numerous major and associated faults. The major faults having a NW-SE trend are the ITSZ, STD, MCT, MBT and HFT extending from north to south. It has also been observed that these major faults along with their associated faults tend to move towards a low-angle northward dipping detachment called the Main Himalayan Thrust (MHT) (Schelling and Arita, 1991).

Our study region is mainly bounded by the ITSZ in the north and by the Indo-Gangetic plain in the south. Along with this, it is also seen that the other three principal thrusts namely MCT, MBT and HFT illustrates the southward migration of the main deformation front due to its young age and shallow depth (Chingtham et al., 2014). The HFT depicts evidence of active deformation zone that is associated with the uplift and active faulting, observed between Sub-Himalaya and the Indo-Gangetic plain. The NW-SE trending and a scarp of discontinuous nature are illustrated by the HFT at a few metres height in the adjoining areas of Pinjor Dun and Dehradun (Thakur and Pandey, 2004). The HFT is well known to have ruptured during large historical earthquakes (Kumar et al., 2003; Javed et al., 2003). However, the Himachal section of the NW Himalaya also consists of many local faults and lineaments (Najman et al., 2004). So the tectonics along with major tectonic discontinuity of our present study area is clearly explained in Fig. 1.

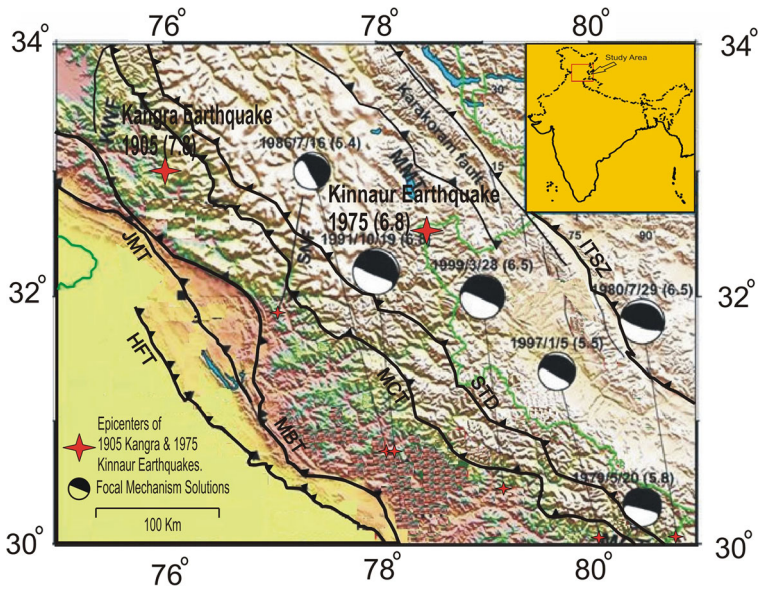

Fig. 1 General tectonic map showing the epicentre of 1905 Kangra earthquake and 1975 Kinnaur earthquake, major tectonic breaks *ITSZ*: Indus-Tsangpo Suture Zone; *MCT*: Main Central Thrust; *MBT*: Main Boundary Thrust; *HFT*: Himalayan frontal thrust; *JMT*: Jawalamukhi thrust; *KWF*: Kishtwar fault; *SNF*: Sundarnager fault; *MMT*: Main Mantle thrust along with the topography as well as the focal mechanism solutions of some major earthquakes that occurred in the region in the past (Modified after Tripathi et al. 2014)

3 Data used and methodology

3.1 Description of network

In the Himachal region, a local seismic network consisting of 12 broadband seismic stations were deployed by WIHG, Dehradun from 2004 around the source region of Kangra earthquake of 1905 of $M_l \geq 7.8$ in a campaign mode. These seismic stations were further upgraded with a seismic array of 10 broadband seismographs in the Sutlej valley, Kinnaur. The broadband seismometer that were operated in the Kangra-Chamba sector was operated since 2004 and the Sutlej valley array was deployed in 2009 around the source region of 1975 Kinnaur earthquake of magnitude $M_l \geq 6.8$. These two arrays were generally deployed to understand the Seismotectonics or the tectonics of the Himachal Himalaya. The array deployed in the Kangra-Chamba sector consists of seismic stations equipped with three-component CMG- 3 T (120 s natural time period). Again the seismic array operated in the Sutlej valley consists of seismic stations that were provided with Trillium-240 broadband sensor having a velocity response between 0.004 to 35 Hz along with 24-bit Taurus digitizer (100 samples/s). Collected data set used was recoded from the year 2004 to 2013. Figure 2 completely illustrates the WIHG Stations deployed in the Himachal Himalaya along with the earthquake hypocentres in the study area. Table 1 completely summarises the station information's used in the network along with the station corrections.

3.2 Data processing

All local events having clear P and S phases are extracted from the raw seed data set of 10 years with the help of the Seisan software (Havskov and Ottemoller, 1999) and filtered with Butterworth filter of frequency range 1–5 Hz. After removing the low- and high-frequency noise from the data, 476 local events having a magnitude range from 1.0 to 5.0 (M_l) were located with the initial reference velocity model of Kumar et al. (2009). We obtained the 1.74±0.03 average Vp/Vs ratio and its standard deviation (Kumar et al., 2009; Mukhopadhyay and Sharma, 2010; Monsalve et al., 2008), which resulted from Wadati's plot using the least square location method for initial epicentre location. But root-mean-square (RMS) residual error associated with the manual picking of the P and S arrival times is up to 0.87 s which is considerably high and gives a sparse distribution of epicentres. This value in RMS misfit can lead to obscured results in the velocity structure and hypocenter locations. So to achieve a best minimal error in the location of the hypocenters out of a total of 476 events, 125 best events with 452 P phases and 937 S phases and least square residual error below 0.40 s were selected for

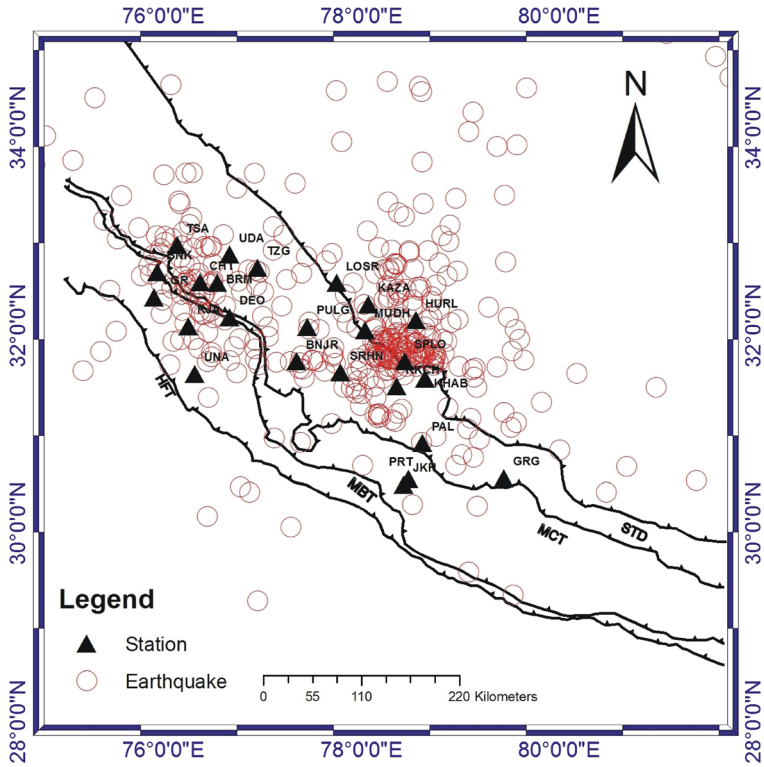

Fig. 2 The Seismic network deployed and operated by Wadia institute of Himalayan Geology, Dehradun (WIHG) along with the seismicity plot in Himachal Pradesh, NW Himalaya, India. The *triangles* indicates the seismic stations and the *hollow red circles* indicates the earthquake epicentres

inversion. This criterion was set to obtain a minimum RMS misfit because there was a huge error associated with the hypocenter location beyond this value that can lead to a systematic biases in the earthquake locations (Jordan and Sverdrup, 1981; Thurber 1992, Billings et al., 1994). Residual error below 0.40 s is used for selecting the best seismic events which is further used for travel time inversion. The minimum 1D velocity model with least square error misfit is derived by applying the inbuilt VELEST package (Kissling. E., 1995)

Table 1 Seismic stations details with station corrections

Station Name	Station code	Latitude (°N)	Longitude (°E)	Elevation (m)	P wave delay	S wave delay
SARHAN	SRHN	31.533	77.792	1,983	−0.050	−0.282
RACKCHHAM	RKCH	31.393	78.356	3,129	−0.070	−0.337
SPILO	SPLO	31.650	78.441	2,353	0.012	−0.216
KHAB	KHAB	31.469	78.644	2,715	−0.031	−0.301
HURLING	HURL	32.062	78.551	3,190	−0.075	−0.397
MUDH	MUDH	31.963	78.038	3,811	−0.104	−0.525
KAZA	KAZA	32.219	78.072	3,701	−0.121	−0.519
LOSSER	LOSR	32.435	77.750	4,141	−0.170	−0.581
PULGA	PULG	31.995	77.452	2,274	−0.100	−0.495
BANZAR	BNJR	31.645	77.348	1,369	0.000	−0.250
DEOL	DEO	32.093	76.672	700	−0.886	−0.283
CHHATRARI	CHT	32.440	76.372	1,800	−0.205	0.844
LAGORE	LGR	32.292	75.907	800	1.504	3.592
UNA	UNA	31.520	76.318	550	0.766	2.551

inside the Seisan software (Havskov and Ottemoller, 1999). Basically, VELEST is a FORTRAN77-based routine program that has been designed to derive 1D velocity models for earthquake location procedures and as initial reference models for seismic tomography (Kissling, 1988; Kissling et al., 1994). This program was originally written by W.L. Ellsworth and S. Roecker for seismic tomography studies in 1976 under the program name HYPO2D (Ellsworth 1977; Roecker, 1981). VELEST has been again modified by R. Nowack and implemented in the layered-model ray tracer by C. Thurber (1981), and R. Comer.

VELEST program is also used to derive the 1D velocity model along with coupled hypocentre solutions. In this, dataset used for VELEST algorithm represents a coupled hypocenter-velocity model problem comprising of the hypocenters, the velocity model and station corrections. Each of such solution may be rated by comparing its corresponding (calculated) travel times with the measured (observed) travel times. These travel time differences are called the misfit (or residuals) of the solution. Mostly, RMS-misfit of the solution is used. To obtain one minimal solution through VELEST algorithm, we have to consider the possible combination of hypocentres, velocity model and station corrections and rate it based on its RMS misfit that would be minimal RMS. So, in this way, VELEST program works for estimating the minimum 1D model and improve the epicentre locations. After deriving the minimum 1D velocity model, the earthquake hypocentres were relocated with the optimised velocity model with an average RMS value of 0.03 s. The obtained average error for preliminary location of these selected events for depth, latitude and longitude is ±3 km. Then the P and S travel time inversion for these selected 125 seismic events is used to derive an optimal 1D velocity model, and these events were also relocated by joint hypocentre determination (JHD) for more refined seismicity within the region.

3.3 Determination of *V*p/*V*s ratio using Wadati's plot

In order to obtain a priori restrain on the velocity model of the region, the Wadati's plot was utilised to estimate the ratio of average P wave velocity to average S wave at different depths and origin time and its variation from the time predicted by the primary locations. Wadati's diagram is a graphical technique that can be used to determine the origin time of an earthquake using P and/

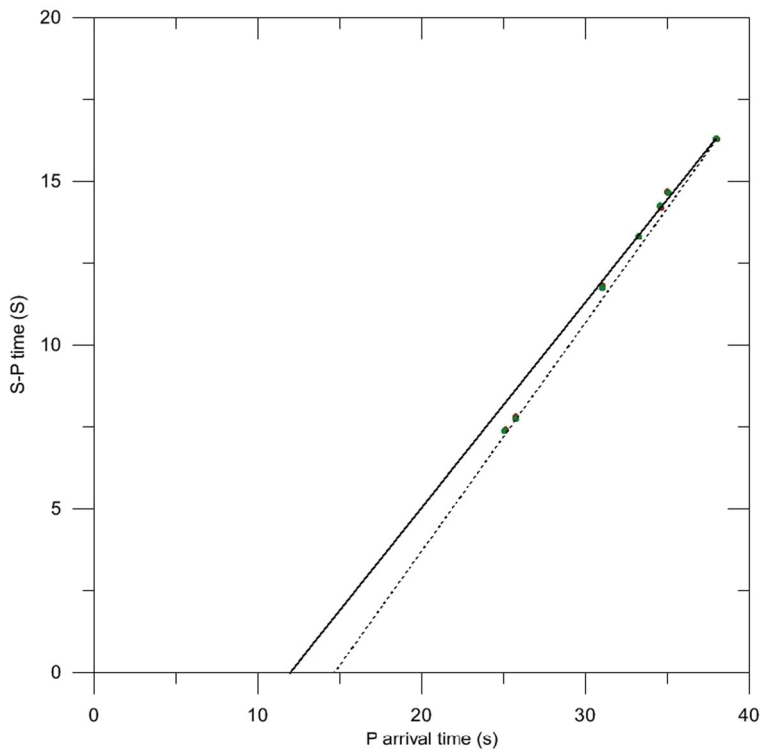

Fig. 3 The two Wadati's plots for a magnitude 5.3 earthquake in Himachal Pradesh in which one is obtained with observed time (*solid line*) arrivals at various recording stations and the other is obtained with predicted time (*dashed line*) arrivals and both are used to obtain a best-fit solution

or S wave arrival time alone. This technique was used by K. Wadati in order to derive the location of deeper earthquakes in seismic bands called Wadati-Benioff zones, which were latter interpreted as seismic events in subducting slabs (Wadati, 1933). The time difference between the arrival of the S wave and the P wave ($t_s - t_p$) is plotted against the absolute arrival time of P wave (Fig. 3). Since the difference between the arrival times of S and P wave goes to zero at the hypocentre, a straight-line fit on the Wadati diagram gives an approximate origin time at the intercept with the P arrival time axis. Figure 3 illustrates two Wadati plots for a magnitude of 5.3 earthquake in Himachal Pradesh in which one is obtained with observed time arrivals at various recording stations and the other is obtained with predicted time arrivals and both are used to obtain a best-fit solution. From Wadati's plot, it is clear that observed S-P time is less than the predicted S-P time which means the real S wave velocity of the area must be less than the one given in Kumar et al. (2009). From this observation, it can also be stated that the real P wave velocity for the area must be less than that given in Kumar et al. (2009). The average Vp/Vs ratio obtained for the region from observed arrivals gives a value of about 1.74 whereas the average Vp/Vs ratio obtained for the region from predicted arrivals gives a value of about 1.77 (Kumar et al., 2009; Mukhopadhyay and Sharma 2010; Monsalve et al., 2008). The deviation in the origin time that intercepts the time axes is 2.6 s. We have again calculated the origin time difference for all the events recorded in the study region and plotted it as a function of depth. Figure 4 clearly indicates that the average P wave velocity should be less than that given in Kumar et al. (2009) for shallower depths up to 30 km. In addition to that, Wadati's plot also depicts a lower Vp/Vs of 1.74 for events at 30 km because for this depth, the difference in origin time is maximum positive i.e. the origin time should be prior to that predicted by the model of Kumar et al. (2009). Figure 4 shows the origin time difference as a function of depth with observed and predicted arrivals. The origin time difference is positive for events at shallower depths up to 30 km which we have considered for velocity inversion and is negative for events at or above 40 km depth.

3.4 Calculation of minimum 1D model from travel time inversion

To obtain an optimal 1D velocity model for the study region, eminent algorithm VELEST (Kissling et al.,

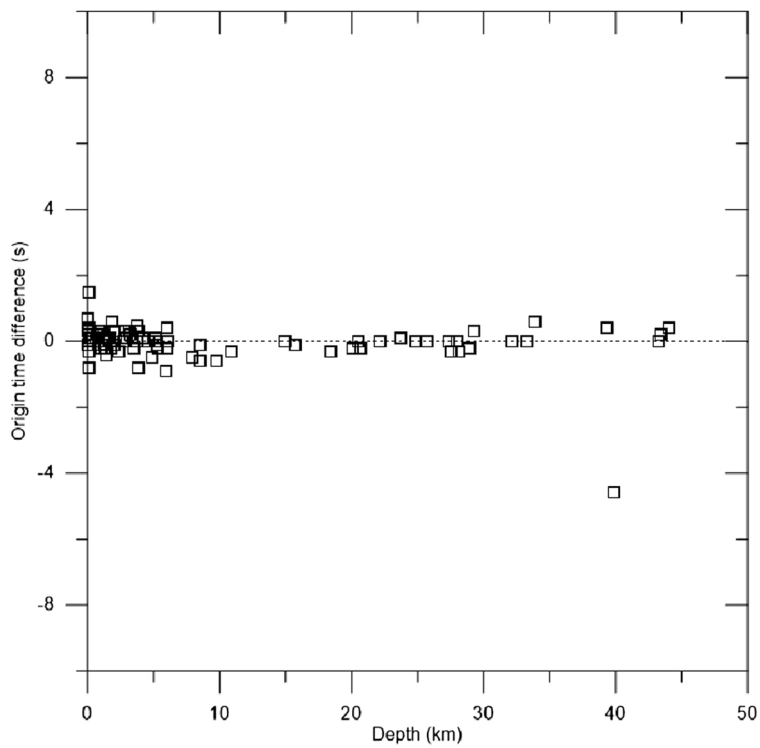

Fig. 4 The origin time difference (*hollow squares*) as function of depth with observed and predicted arrivals obtained for the study region

1984; Kissling, 1988) has been used. This algorithm is highly efficient and widely accepted for calculating the crustal velocity structure in the tectonically complex and seismically active areas around the globe (Haslinger et al., 1999; Ojeda and Havskov, 2001; Langer et al., 2007). With this approach, we have deduced hypocentre locations, 1D crustal structure and station corrections by the simultaneous inversions of travel time data along with least square residual error. We have used a total of 125 seismic events contained 452 P phases and 937 S phases, lying within the array having a higher accuracy in hypocentre parameters for travel time inversion and calculation of minimum 1D crustal model. The seismic events with at least 6 P phases and 6 S phases are selected for inversion. We have taken the model of Kumar et al. (2009) as a preliminary reference model for the computation of a least 1D velocity model which is given in Table 2. After five iterations, we have obtained an optimal 1D velocity model with a least square residual error of 0.03 s as minimum and maximum up to 0.24 s which was initially maximum up to 0.40 s before the iterations. This shows that the optimal model obtained from this algorithm is of higher accuracy compared to the initial reference model. In this process, maximum seismic events lie within 30 km depth, which are able to provide the high accuracy crustal structure for this depth.

4 Results

4.1 Optimal 1D velocity model for Himachal Himalaya

The optimal 1D velocity model is achieved by inverting the earthquake epicentres along with earlier published velocity model of P and S wave for the study region. Here we have studied to obtain a result based on the least square residual error and also make sure that all the results derived clearly matched with the previous information obtained from initial locations. We started our first inversion on the basis of the initial model of Kumar et al. (2009) for the NW Himalaya. We changed the preliminary model in successive trials till obtained smaller misfits. After five successful iterations, we observed that the RMS values are constant at lower than 0.03, meaning that it is the final result. The obtained RMS residual for arrival time of the events with the new velocity model showed a dramatic decrease of earlier maximum of 0.40 to 0.24 s. i.e. the velocity model is highly accurate and can significantly explain the crustal structure variations of the study region. Thus the minimum 1D velocity model is obtained from travel time inversion of P and S waves. This velocity model divides the 30 km crustal layer into seven layers with a velocity of 5.314 km/s for the topmost layer (up to 5 km) and of 5.391 km/ for the second layer (up to 10 km). There is a slight change from 5.391 km/s at 10 km to 5.392 km/s i.e. 0.01 km/s at 15 km depth that is significantly low but there is a major change in velocity from 5.392 km/s at 15 km to 5.964 km/s at 20 km depth suggesting that Conrad discontinuity is at 18 km depth within the crust i.e. a sharp velocity contrast thus marking the boundary between Sial and Sima. This generally matches with the tectonics of the area which suggests that crust has shallow seismic events that are mainly confined at upper crustal layer. Table 3 describes the minimum 1D model obtained with VELEST algorithm by inverting the P and S wave arrival times. Figure 5(a) shows the least square residual 1D P wave velocity model obtained through VELEST and its comparison plot with the preliminary velocity model of Kumar et al. (2009) and Kamble et al. (1974) and Fig. 5(b) shows the obtained minimum 1D S wave velocity model and its comparison plot with the other two initial models.

Table 2 Preliminary velocity model of Kumar et al., 2009

Depth (km)	P wave velocity (km/s)	S wave velocity (km/s)
0	5.27	3.01
10	5.55	3.21
15	5.45	3.05
18	6.24	3.59
46	8.25	4.73

Table 3 Final velocity model obtained through VELEST

Depth (km)	P wave velocity (km/s)	S wave velocity (km/s)
0	5.219	2.998
5	5.314	3.015
10	5.391	3.134
15	5.392	3.135
20	5.964	3.441
25	6.071	3.482
30	6.313	3.647

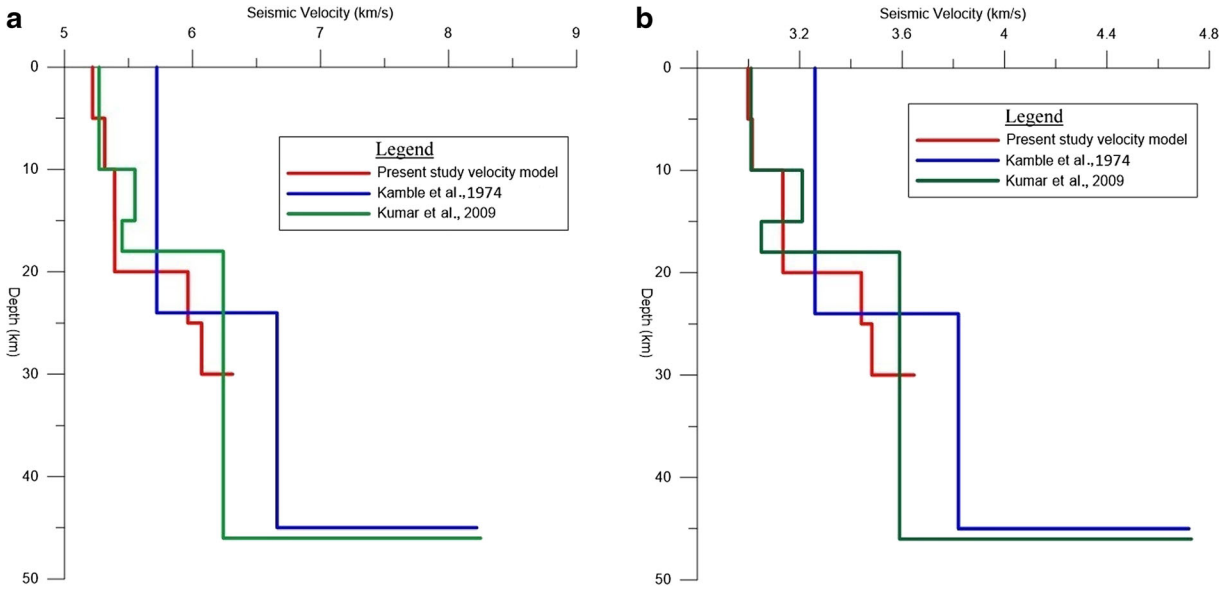

Fig. 5 **a, b** The minimum 1D velocity model of seven layers (*red line*) obtained with VELEST from travel time inversion of P and S wave arrival times and its comparison plot with the preliminary velocity of Kumar et al. 2009 (*green line*) and Kamble et al., 1974 (*blue line*)

4.2 Improved RMS for earthquake hypocentres

The velocity model obtained with VELEST has considerably reduced the least square residual error in hypocentre location from 0.40 s maximum to 0.24 s and the lowest least square residual error obtained after relocating the events with VELEST is 0.03 s, which is very rarely seen with other data sets. This illustrates that the earthquake epicentre location parameters obtained with inversion are highly accurate for the study region.

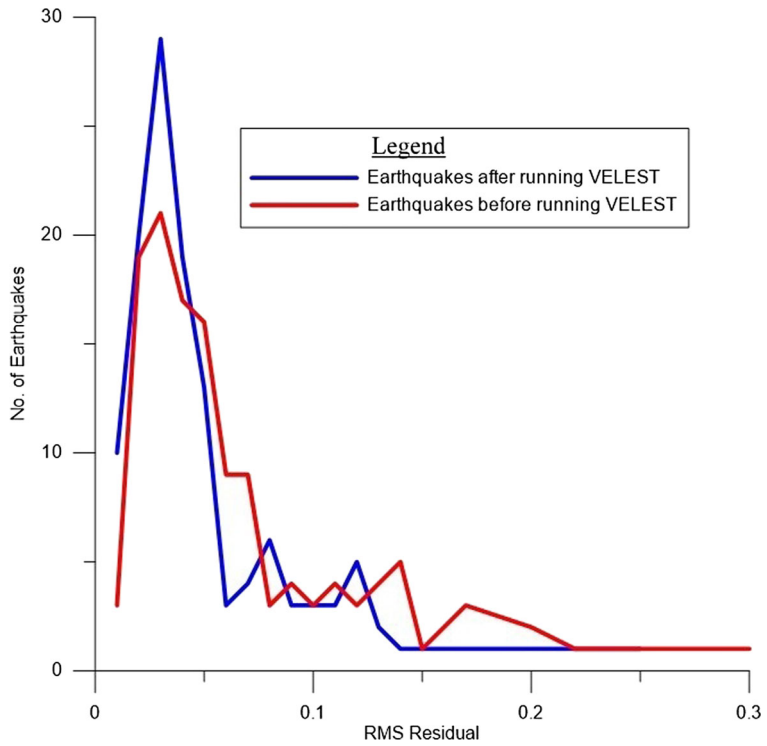

Fig. 6 Shows a comparison between the RMS values with respect to number of earthquakes obtained for the Hypocentres before applying the VELEST (*red line*) algorithm and after (*blue line*) applying it. This shows a gradual decrease in minimum and maximum RMS residual values after VELEST is applied

To check the stability of the obtained model we have broken again the initial model at 3.5 and 4.0 km intervals with certain assumed velocity. While inverting, these two models converge and match with same least square residual of earlier obtained value. The starting velocity for both the iteration models were same with the velocity of Kumar et al. (2009). These velocities were varied in subsequent runs and down the RMS misfits. By conducting this test, there is a negligible variance in the velocity value at subsequent layers. Finally, we have combined these two models to obtain our final model. This final velocity model shows a variation in the velocity of P and S at subsequent layers is the optimal velocity model. The used events are maximally concentrated up to 30 km depth in this study. Therefore, this velocity model has been proposed mainly for the upper crustal layer. Final velocity model occurs due to the presence of maximum number of events having lowest RMS which shows that the obtained model is highly stable and can be used extensively for earthquake hypocentre location. Figure 6 shows a significant decrease in RMS residual values after locating the selected subset of 125 events with VELEST in comparison to the epicentres located previously with routine epicentre location software. Figure 7a, b show two iteration models and the final obtained model in Fig. 7c with their RMS residuals computed against the total number of earthquakes in the study region.

4.3 Variations in lateral velocity and station corrections

The obtained least square residual 1D velocity model is used for computing the JHD (Joint Hypocenter determination) and station corrections by the method of VELEST algorithm. The station correction is defined as a parameter for velocity deviation from optimal 1D velocity model. Thus, station corrections for 14 stations out of 22 stations in this network were calculated and given in tabular form in Table 1. The stations lying in the borderline are ignored for calculation of station corrections. Calculated station corrections are then plotted in the form of contours with different values. These station corrections are computed taking into consideration the PULG station as the reference station as it lies almost at centre of the network. We obtained positive variation in station corrections for P waves from −0.8856 at DEO to 1.5044 at LGR and from −0.5807 at LOSR to 3.5929 at LGR for S waves. These variations are resemblance to the 3 D nature of the velocity in the study region. Positive variations are observed where the actual velocity is less than the predicted one and vice versa. The negative values of the station correction deciphers the possibility of a deeper velocity variation. This marks the presence of overriding wedge which occurs due to increase in thickness of the crust. Figure 8a, b completely

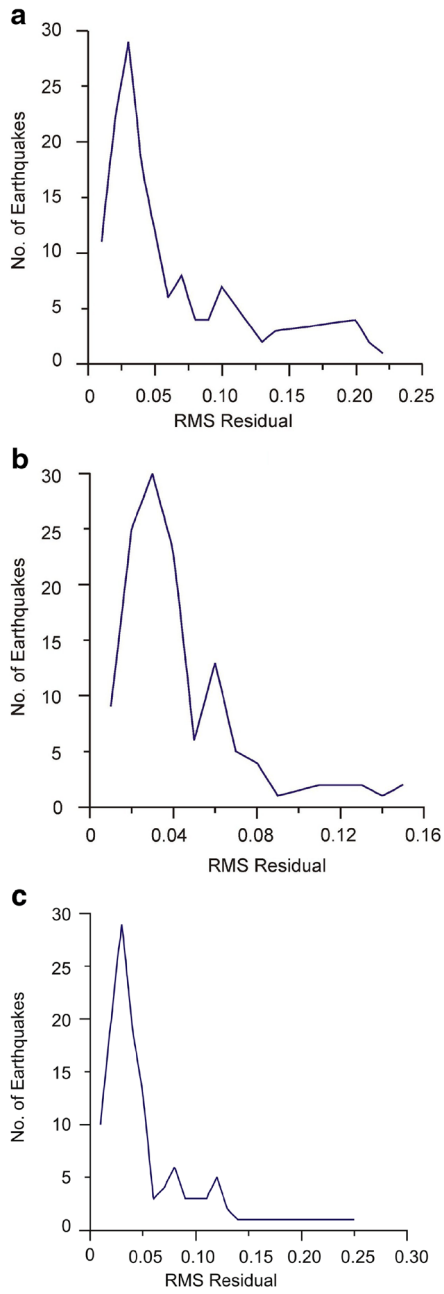

Fig. 7 **a**, **b**, **c** The number of earthquake hypocentre and its variation with the RMS residual (*blue line*) for the two iteration velocity models at an interval of 3.5 km, 4.0 km and for the final obtained model at an interval of 5.0 km

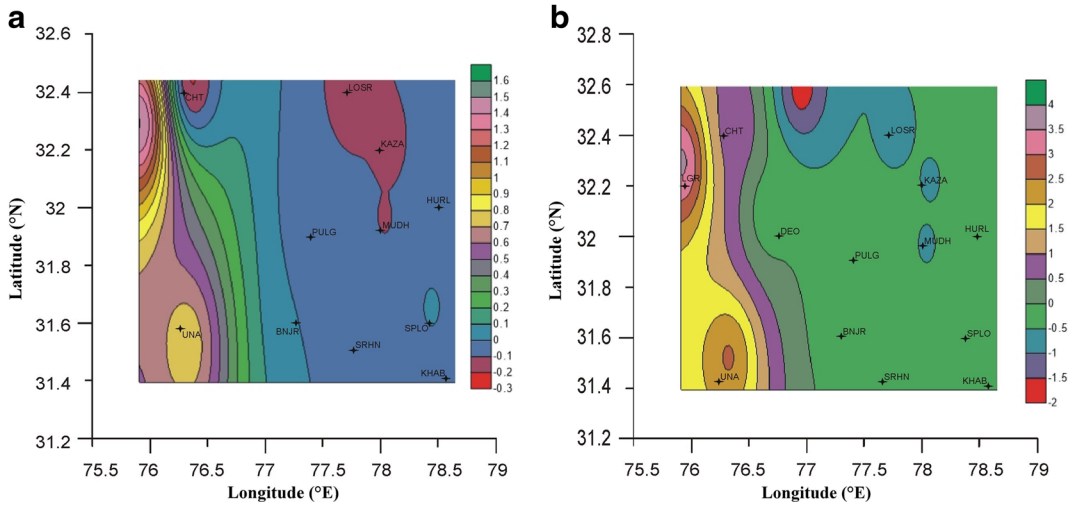

Fig. 8 **a**, **b** The variation of station corrections with respect to P delay and S delay by taking PULG station as the reference station. *Solid black star* indicates seismic stations

depict the contour map of P and S delay at various stations lying within the array by considering PULG as the reference station.

4.4 Seismicity study and JHD

The JHD computed by including the station corrections resulted in the relocation of hypocentres with higher precision and accuracy. A total of 125 seismic events were considered for travel time inversion, the overall least square residual error reduced from a minimum of 0.03 s to 0.01 s and the errors significantly related with Hypocentre determination reduced to ± 1 km. Figure 9a, b show the spatial distribution of seismic events within the array after taking station corrections into account. The depth distribution of a large number of earthquake hypocentres lies between the range of 0 and 10 km range, and a maximum up to 60 km that implies the presence of maximum shallow seismicity in the region. Mainly the events are more clustered in the area lying between latitude 31.0 °N to 32.8 °N and 76.8 °E to 78.8 °E, which shows high seismotectonic activity in the area due to the strain accumulation caused by dipping of Indian plate under the Eurasian plate. It is also inferred

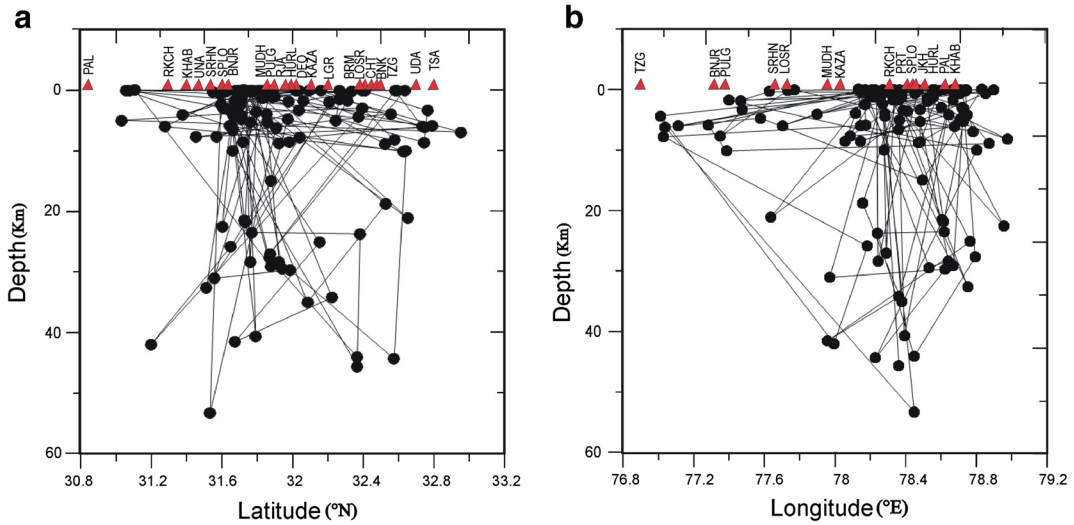

Fig. 9 **a**, **b** The Ray path coverage of the seismic events to reach different stations with respect to latitude and longitude. *Solid black circles* indicates earthquake hypocenters and *solid red triangles* shows recording stations

from earlier studies that high concentration of seismic events in this region are due to compressive environment that signifies thrust mechanism of fault orientation which completely agrees with the tectonics of the region.

The shifting of the earthquake epicentres which were located with the help of new 1D velocity model was observed when again the data was relocated with the help of the JHD technique. This is illustrated by the Fig. 10. There is not much shifting of the epicentres which show that 1D model obtained for the region is highly reliable for advanced tomographic study.

5 Discussion and conclusions

The seismic events recorded through the local network were used to derive the velocity structure of the region by travel time inversion of P and S waves, respectively. Due to shallow seismic activity in the region, the arrival times could only calculate the upper crustal velocity up to 30 km with more precision. This further gives the inference that the first discontinuity in this region lies at 18 km depth. So, this crustal part of the Himalaya is quite thicker as compared to other Himalaya parts. According to earlier studies by Hazarika et al. (2013) and our study, we can suggest that the Moho depth in this part of the Himalaya lies approximately between 50 and 60 km. The Vp/Vs ratio inferred from Wadati's plot gives a value of 1.74 with a standard deviation of 0.03 s which is globally supported by earlier published results (Kumar et al., 2009; Mukhopadhyay and Sharma 2010; Monsalve et al., 2008). While putting cross section across the known thrust faults namely MBT, MCT and STD, we observed that the seismicity at MCT is mostly controlled by seismic activity taking place along these thrust faults and the maximum depth of the seismic events are restricted up to 30 km depth. Then, we see towards the north of the MCT the depths of the seismic events increase with effect of both MCT and STD faults. The seismic activity across the STD fault is high that is mainly controlled by the India-Eurasia collision. The cross section across the major thrust faults also coincide with the Kaurik-Chango Fault (KCF)—a normal fault having an N-S dip. The maximum seismicity lies both sides of the STD across the Kaurik fault which is responsible for the neotectonic activity (Joshi et al., 2010). In view of this, the teleseismic tomography using

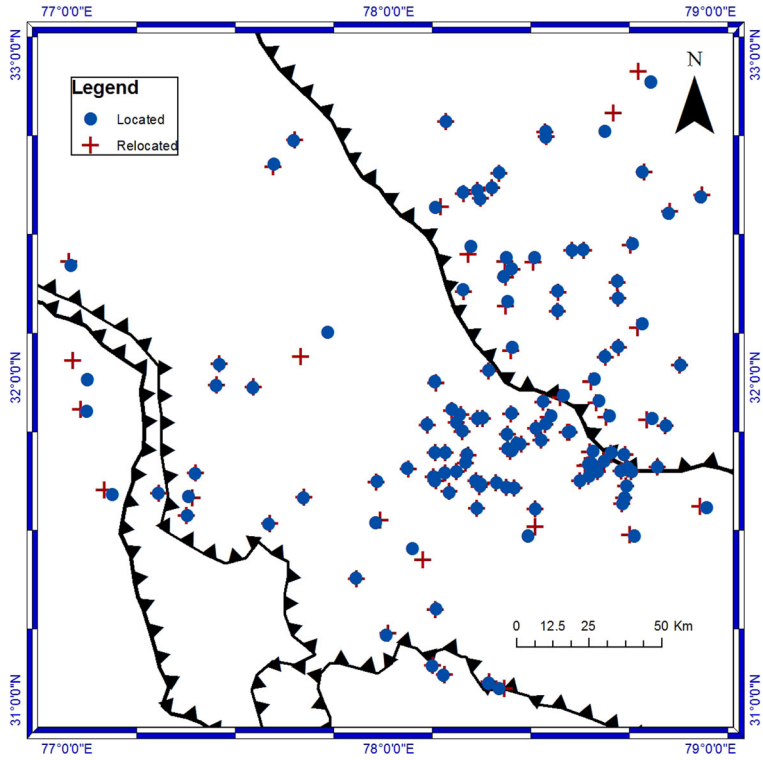

Fig. 10 Shows epicentral location (*solid blue circles*) of the earthquakes with the new 1D velocity model and again its relocation (*solid red cross*) by using the JHD technique across the various tectonic faults, such as *MCT*: Main Central Thrust; *MBT*: Main Boundary Thrust; and *STD*: South Tibetan Detachment

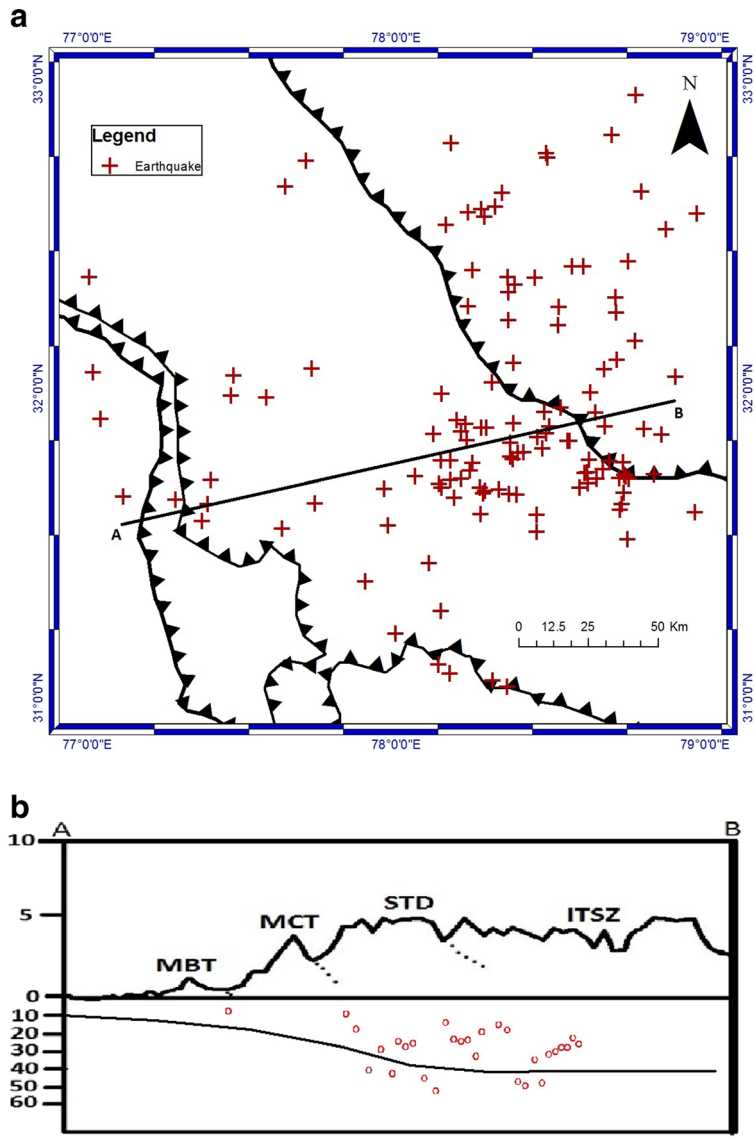

Fig. 11 **a** The transect AB (*solid black line*) taken across in the WWS-EEN direction cutting through major thrusts staring from *MBT* (Main Boundary Thrust) in north to *STD* (South Tibetan detachment) in South. The major thrust faults through which the transect pass are termed as MBT, MCT, STD from south to north. The earthquake epicentres are indicated by *solid red cross* symbol. **b** The focal depth distribution of seismic events (*hollow red circles*) across major tectonic boundaries. Such as *MBT*: Main Boundary Thrust; *MCT*: Main Central Thrust; *STD*: South Tibetan Detachment; *ITSZ*: Indus-Tsangpo Suture Zone; from south to north (Modified after Hazarika et al. 2013)

receiver function analysis may be able to infer the crustal structure up to more depth and also suggests the discrepancy of Moho depth more accurately in this study region. Through process of travel time inversion, we have found a new highly active seismic window lying in the latitude range of 31.8 °N to 32.8 °N and longitude range of 76.8 °E to 78.8 °E along with the previously active region for the Kangra earthquake of 1905 and Kinnaur earthquake of 1975 that indicates high tectonic activity in this part of the Himalaya.

Due to this, we have cut across the major faults in the region starting from MBT to STD shown in Fig. 11a, b completely summarising the depth distribution of events along various thrusts cut through the transect AB. There are also some new faults and lineaments along with the major thrust faults of MBT, MCT, STD and ITSZ to account for the increased seismic activity in this region in recent years. So, the optimal 1D velocity model calculated here is highly efficient to be used as an input model for local 3D tomography in future.

Acknowledgments We are very much grateful to Director Wadia Institute of Himalayan Geology, Dehradun for giving permission to publish this work. We also heartily acknowledge Prof. Anil Kumar Gupta for the needful help in editing the manuscript. The authors of the Manuscript are also extremely grateful to Prof. Yu Jeffrey Gu, Associate Professor of Geophysics, University of

Alberta (USA) and Associate editor for Journal of seismology for thoroughly reviewing the manuscript and providing his valuable suggestions towards improving the manuscript. Shri. R.S. Negi is highly acknowledged for the support and encouragement during the manuscript preparation. Mr. Tarun Jain is acknowledged for his help in redrawing some of the figures for the manuscript. All other supporting staffs of Geophysics group and institute are acknowledged for their fruitful help in data collection in very tough conditions in Himalaya.

References

Billings SD, Sambridge MS, Kennett BLN (1994) Error in hypocentre location: picking, model, and magnitude dependence. Bull Seismol Soc Am 84:1978–1190

Bollinger L, Avouc JP, Cattin R, Pandey MR (2004) Stress buildup in the Himalaya. J Geophys Res 109:1–8

Chingtham P, Chopra S, Baskoutas I, Bansal BK (2014) An assessment of seismicity parameters in northwest Himalaya and adjoining regions. Nat Hazards 71:1599–1616

Ellsworth, WL (1977) Three-dimensional structure of the crust and mantle beneath the island of Hawaii. Ph D thesis, MIT, Massachussetts, USA.

Gaur VK, Chander R, Sarkar I, Khattri KN, Sinvhal H (1985) Seismicity and state of stress from investigations of local earthquakes in the Kumaun Himalaya. Tectonophysics 118: 243–251

Haslinger F, Kissling E, Ansorge J, Hatzfeld D, Papadimitriou E, Karakostas V, Makropoulos K, Kahle HG, Peter Y (1999) 3-D crustal structure from local earthquake tomography around the gulf of Arta (Ionian region, NW Greece). Tectonophysics 304:201–218

Havskov J, Ottemoller L (1999) Seisan earthquake analysis software. Seismological research. Letters 70(5):532–534

Hazarika D, Kumar N, Yadav DK (2013) Crustal thickness and Poisson's ratio variations across the northwest Himalaya and Eastern Ladakh. Acta Geophys 61:905–922

Javed NM, Nakata T, Philip G, Virdi NS (2003) Preliminary observations from trench near Chandigarh, NW Himalaya and their bearing on active faulting. Curr Sci 85:1793–1798

Jordan TH, Sverdrup KA (1981) Teleseismic location techniques and their application to earthquake clusters in the South-Central Pacific. Bull Seismol Soc Am 71:1105–1130

Joshi M, Kothyari GC, Ahluvalia A, Pant PD (2010) Neotectonic evidences of rejuvenation in Kaurik-Chango Fault Zone, Northwestern Himalaya. J Geogr Inf Syst 2:169–176

Kamble VP, Verma RK, Choudhury HM (1974) Crustal structure in Dalhousie-Mandi section of the Himalayan foothills. Part I. Indian J Meteorol Geophys 25:229–236

Kayal JR (2001) Microearthquake activity in some parts of the Himalaya and the tectonic model. Tectonophysics 339:331–351

Kayal JR, Ram S, Singh OP, Chakraborty PK, Karunakar G (2003) Aftershocks of the March 1999 Chamoli earthquake and seismotectonic structure of the Garhwal Himalaya. Bull Seismol Soc Am 93:109–117

Khattri KN, Chander R, Gaur VK, Sarkar I, Kumar S (1989) New seismological results on the tectonics of the Garhwal Himalaya. Proc Indian Acad Sci Earth Planet Sci 98:91–109

Khattri KN, Tyagi AK (1983) Seismicity patterns in Himalayan plate boundary and identification of the areas of high seismic potential. Tectonophysics 96:281–297

Kissling E (1988) Geotomography with local earthquake data. Rev Geophys 26:659–698

Kissling E (1995) Program VELEST User's guide—short introduction (second draft version). Institute of Geophysics and Swiss Seismological Service, ETH-Hoenggerberg, Zurich, pp 1–26

Kissling E, Ellsworth WL, Cockerham RS (1984) Three dimensional structure of the long Valley Caldera, California region by geotomography. U.S. Geol. Surv. Open-File Rep 84–939: 188–220

Kissling E, Ellsworth WL, Eberhart-Phillips D, Kradolfer U (1994) Initial reference models in local earthquake tomography. J Geophys Res 99:19635–19646

Kumar S, Wesnousky SG, Rockwell TK, Thakur VC, Seitz GG (2003) Earthquake recurrence and rupture dynamics of Himalayan frontal thrust, India. Science 294:2328–2331

Kumar N, Sharma J, Arora BR, Mukhopadhyay S (2009) Seismotectonic model of the Kangra–Chamba sector of Northwest Himalaya: constraints from joint hypocentre determination and focal mechanism. Bull Seismol Soc Am 99: 95–109

Langer H, Raffaele R, Scaltrito A, Scarfi L (2007) Estimation of an optimal velocity model in the Calabro-Peloritan mountains assessment of the variance of model parameters and variability of earthquake locations. Geophys J Int 170:1151–1164

Monsalve G, Sheehan A, Rowe C, Rajaure S (2008) Seismic structure of the crust and the upper mantle beneath the Himalayas: evidence for eclogitization of lower crustal rocks in the Indian plate. J Geophys Res 113:B08315–B08330

Mukhopadhyay S, Sharma J (2010) Crustal scale detachment in the Himalayas: a reappraisal. Geophys J Int 183:850–860

Najman Y, Johnson K, White N, Grahame O (2004) Evolution of the Himalayan foreland basin, NW India. Basin Res 16:1–24. doi:10.1111/j.1365-2117.2004.00223.x

Ni J, Barzangi M (1984) Seismotectonics of the Himalayan collision zone D geometry of the underthrusting Indian plate beneath the Himalaya. J Geophys Res 89:1147–1163

Ojeda A, Havskov J (2001) Crustal structure and local seismicity in Colombia. J Seismol 5:575–593

Pandey M, Tandukar R, Avouac J, Lave J, Massot J (1995) Interseismic strain accumulation on the Himalayan crustal ramp (Nepal). Geophys Res Lett 22:751–754

Roecker SW (1981) Seismicity and tectonics of the Pamir-Hindu Kush region of central Asia, Ph.D. thesis, Mass. Inst. of Technol., Cambridge.

Schelling D, Arita A (1991) Thrust tectonics, crustal shortening and the structure of the fareastern Nepal Himalayas. Tectonics 10:851–862

Srivastva HN, Dube RK, Raj H (1986) Space and time variation in seismicity patterns preceding two earthquakes in the Himachal Pradesh, India. Tectonophysics 138:69–77

Thakur VC, Rautella P, Jaffaruddin M (1995) Normal faults in Panjal thrust zone in lesser Himalaya and between higher Himalayan crystallines and Chamba sequence in Kashmir Himalaya. India Proc Indian Acad Sci (Earth Planet Sci) 104:499–508

Thakur VC, Pandey AK (2004) Active deformation of Himalayan frontal thrust and piedmont zone south of Dehradun in respect of seismotectonics of Garhwal Himalaya. J Himal Geol 25:25–31

Thurber CH (1981) Earth structure and earthquake locations in the Coyote Lake area, central California, Ph.D. thesis, Mass. Inst. Technol.

Thurber CH (1992) Hypocenter-velocity structure coupling in local earthquake tomography. Phys Earth Planet Sci Lett 75:55–62

Tripathi JN, Singh P, Sharma ML (2014) Attenuation of high-frequency P and S waves in Garhwal Himalaya, India. Tectonophysics 636:216–227

Wadati K (1933) On the travel time of earthquake waves. Part II. Geophys Mag 7:101–111